Protein Flexibility and Conformational State: A Comparison of Collective Vibrational Modes of Wild-Type and D96N Bacteriorhodopsin

S. E. Whitmire,* D. Wolpert,* A. G. Markelz,* J. R. Hillebrecht,[†] J. Galan,[†] and R. R. Birge[†]

*Physics Department, University at Buffalo, State University of New York, Buffalo, New York; and [†]Departments of Chemistry and of Molecular and Cell Biology, University of Connecticut, Storrs, Connecticut

ABSTRACT   Far infrared (FIR) spectral measurements of wild-type (WT) and D96N mutant bacteriorhodopsin thin films have been carried out using terahertz time domain spectroscopy as a function of hydration, temperature, and conformational state. The results are compared to calculated spectra generated via normal mode analyses using CHARMM. We find that the FIR absorbance is slowly increasing with frequency and without strong narrow features over the range of 2–60 cm^{-1} and up to a resolution of 0.17 cm^{-1}. The broad absorption shifts in frequency with decreasing temperature as expected with a strongly anharmonic potential and in agreement with neutron inelastic scattering results. Decreasing hydration shifts the absorption to higher frequencies, possibly resulting from decreased coupling mediated by the interior water molecules. Ground-state FIR absorbances have nearly identical frequency dependence, with the mutant having less optical density than the WT. In the M state, the FIR absorbance of the WT increases whereas there is no change for D96N. These results represent the first measurement of FIR absorbance change as a function of conformational state.

INTRODUCTION

To understand protein interactions, it is critical to determine the role of conformation state and protein flexibility. Changes of state, photobleaching, and photocycling often involve subtle changes in tertiary structure. A given conformational change can often be decomposed into the collective vibrational modes that would constitute such a motion. Conformational vibrational modes are distinct from the familiar mid-infrared or infrared vibrational modes, which in general involve the motion of only pairs or small groups of molecules. Conformational modes involve the collective motion of entire subunits of the protein with 50–100 atoms moving in concert. These modes lay in the far infrared (FIR) with frequencies between 1 and 200 cm^{-1} (Brooks et al., 1988). We can then quantify conformational flexibility in terms of the density and spectrum of these low-frequency collective vibrational modes.

Characterization of protein conformational flexibility through the measurement of collective vibrational modes has been attempted by using inelastic neutron scattering (INS) (Diehl et al., 1997; Doster et al., 1989; Ferrand et al., 1993), Raman (Urabe et al., 1998; Weidlich and Lindsay, 1988; Weidlich et al., 1990a), and FIR studies (Genzel et al., 1984; Lindsay et al., 1988; Lisy et al., 1997; Markelz et al., 2000; Powell et al., 1987, 1991; Weidlich et al., 1987, 1990b; Wittlin et al., 1986). For bacteriorhodopsin (BR), Raman measurements have mainly examined the collective modes of the attached retinal chromophore with modes $\nu > 200$ cm^{-1}. Conformational modes of the BR polypeptide have been studied using INS (Ferrand et al., 1993; Zaccai, 2000). These studies of wild-type (WT) BR as a function of temperature and hydration show a broad response without

identifiable modes. No conformational state measurements were performed with INS to date.

FIR measurements of proteins have been more limited due in part to the need to use Fourier transform infrared systems coupled with cryogenic detection. In this frequency range, one needs to minimize liquid water (which has a large absorption coefficient in the FIR) but sufficiently hydrate the sample for bioactivity, native conformation. Recently, however, a time-resolved FIR measurement was performed suggesting a 115 cm^{-1} collective mode lifetime >500 ps (Xie et al., 2002). Very low-frequency (1–40 GHz) measurements have been performed using microwave absorbance measurements(Birge et al., 1996; McIntosh and Boucher, 1991). Because the frequency range is below that for excitation of collective modes, the observed absorbances are associated with charge transport events.

FIR absorbance measures only optically active modes with absorbance spectrum A given approximately by $A = \int f(\nu)g(\nu)d\nu$, where $g(\nu)$ is the density of normal modes for a given conformation, and $f(\nu)$ is the oscillator strength for mode ν. Our FIR absorbance measurements are performed using terahertz time domain spectroscopy (TTDS) systems that use ultrafast optical or near-infrared (NIR) solid-state lasers to both generate and detect the terahertz light and offer a number of distinct advantages over standard FIR spectroscopy techniques. These are, mainly, ease of use, time-resolved measurement, access to the real and imaginary part of the dielectric constant, and bandwidth from 2 to 100 cm^{-1}. A number of authors have applied TTDS to biophysical systems including: imaging for diagnosis of tissue damage and dental decay (Han et al., 2000; Longbottom et al., 2002) spectroscopy for biomolecular identification (Brucherseifer et al., 2000; Nagel et al., 2001; Woolard et al., 1997), and conformation determination (Markelz et al., 2000; Walther et al., 2000). To our knowledge, no measurements have examined how confor-

---

mational change affects these modes. In this report, we present FIR absorbance measurements of the collective vibrational mode spectrum for WT and the D96N mutant bacteriorhodopsin in both illuminated and nonilluminated environments. This is the first demonstration of how FIR absorbance measurements can be used to detect changes in the tertiary structure of a biomolecule.

BR is a transmembrane protein (26 kDA) that is native to an archaebacteria known as *Halobacterium salinarum* (Lanyi, 1999). Archaebacteria are an evolutionarily distinct domain of organisms that are known to thrive in extreme environments. Such environments include underwater hydrothermal vents, salt marshes, hot springs, and obsidian pools. *H. salinarum* exists in hypersaline environments known to have NaCl concentrations that are six times that of seawater (~0.6 M) (Stuart and Birge, 1996). Under conditions of low oxygen tension and high light intensity, BR will enable the organism to generate energy via photosynthesis rather than through aerobic metabolism. A retinal cofactor (chromophore), which is responsible for the purple color of the protein, is attached to the protein via a protonated Schiff base linkage to K216 to form a quadrupole with two negative (D85, D212) and one positive counterion (R82) (Kusnetzow et al., 1999). Femtosecond photoisomerization of this chromophore represents the primary photochemical event (Stuart and Birge, 1996). Light excitation of the chromophore activates a photocycle consisting of a series of intermediate states, known as J, K, L, M, N, and O. Each intermediate is characterized by its unique UV/Vis absorbance as shown in Fig. 1. The primary event of the light-adapted species is characterized by an isomerization from the all-*trans* to 13-*cis* conformation. This isomerization along with key interactions taking place between the chromophore and residues lining the retinal binding pocket lead to the transport of a proton from the cytoplasmic to extracellular face of the membrane. The continual photocycling of protons creates a potential gradient that is used to drive the formation of ATP through a series of external chemical reactions. Each intermediate state is associated with a thermal change in the conformation of retinal with its surrounding protein environment. A key conformational change occurs with the L → M transition in which the residue D85 becomes protonated, and the retinal Schiff base becomes deprotonated (Lanyi and Pohorille, 2001). It is believed that numerous conformational changes occur during the lifetime of the M state due to the need for

the retinal chromophore to interact with both the proton acceptor and donor groups. This investigation is focused on observing change in FIR absorbance with the M state as well as the temperature and hydration dependencies. We find that, despite having nearly identical ground-state FIR absorbance, the WT FIR absorbance increases as a function of conformational change, whereas the D96N mutant does not. If we interpret the strength of the absorbance as related to the conformational flexibility, this result is consistent with the three-order-of-magnitude increase in photocycling time of D96N relative to WT. Thus, the significant increase in the M-state lifetime of D96N may be due in part to conformational flexibility within the WT protein, as well as a decrease in the efficiency of proton donation to the binding site for D96N.

MATERIALS AND METHODS

Bacteriorhodopsin is isolated in the form of purple membrane patches (Oesterhelt and Stoeckenius, 1974). These patches consist of ~25% lipid and 75% protein. We found the uniformity of the films to be critical for the THz measurements. This uniformity was achieved using the following protocol. Solutions of BR were spun down to pellet form (35 min at 32 K rpm), dissolved in doubly deionized water, and sonicated for 1 h to fully dissolve aggregates. A 2% glycerol solution of the sonicated media was pipetted onto the substrate and rapidly dried in a dessicant box that was constantly purged with dry nitrogen gas. One half of the substrate was left clean to be used as a reference. The protein films had thicknesses of roughly 200 μm and optical densities of A_{568} ~1–3. There were a total of three WT samples and three D96N samples measured.

For the initial FIR absorption measurements, conditions were set to capture the M intermediate state, which has a lifetime of ~10 ms at room temperature and pH 7. It has been shown that the stability of the M state can be prolonged indefinitely at 233 K (Sass et al., 1997). Below 233 K, BR can no longer photocycle, possibly due to the molecule's inability to access the necessary conformations, as suggested by INS results (Ferrand et al., 1993; Zaccai, 2000). Thus by cooling the sample to 233 K and illuminating with $\lambda > 570$ nm, the change in the FIR absorbance due to the induced M state population can be measured in equilibrium. A temperature-controlled hydration cell was used to both maintain the required temperature and hydration for M state capture and photocycling. The sample holder is in contact with a temperature-controlled stage consisting of a Peltier cooler mounted on a fluid heat exchange platform. Cold nitrogen gas was used as heat exchange fluid. The quartz sample slides are mounted on a brass holder with two 4-mm diameter identical apertures, one aperture over the BR-coated side of the substrate, the other aperture over the uncoated side of the substrate, which is used as a reference. A thermocouple is mounted on the brass sample holder directly next to the quartz sample slide. The holder is surrounded by a closed cell with polypropylene windows. The relative humidity in the cell is controlled by flushing the cell with air pumped over a saturated salt solution. The typical time for flushing before data taking was

bR 568 nm ⇔ K 610 nm ⇔ L 550 nm ⇔ M 410 nm ⇔ N 560 nm ⇔ O 640 nm ⇔ bR 568nm
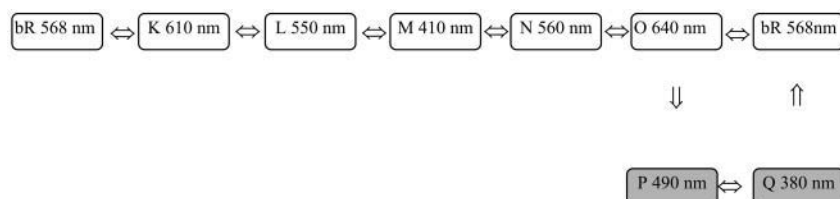
⇓   ⇑

P 490 nm ⇔ Q 380 nm

FIGURE 1 Photocycle of bacteriorhodopsin. Note that the relaxed state of BR is denoted as bR.

>2 h. Hydration equilibration times for OD 1 BR films is ~1 h (Varo and Keszthelyi, 1983). During cool down, the pump was turned off and the input/output lines were sealed to prevent condensation on the sample. Repeated measurements of the FIR transmission through the reference and sample by toggling the hydration cell between the reference substrate aperture and the BR film aperture reduces affects of laser drift, and removes rotational water lines due to the gas phase water in the hydration cell as well as any absorption due to condensed liquid water on the substrate. The temperature and conformational dependence of the THz absorption was determined by thermal cycling and photocycling the samples. THz absorbance was measured at room temperature and again after the sample was cooled to 233 K in the dark. The sample was then illuminated with a 480 nm low-pass filtered white light for 45 min and intermediate state content was monitored with the UV/Vis absorbance. The intermediate state THz absorbance was measured. To check for reproducibility, THz measurements were performed again after the cooled sample was illuminated with white light for conversion back to ground state and then after the sample returned to room temperature. The THz absorbance after white light illumination was the same as the initially cooled 233 K dark measurement and the initial and final room temperature measurements were the same.

The optical set up for the FIR measurements using TTDS is shown in Fig. 2. We use an unamplified Ti-Sapphire mode locked laser with $\lambda = 790$ nm, pulse width of 65 fs, and average power of 300 mW as our ultrafast NIR source for THz generation and detection. THz pulses are generated using photoconductive switches embedded in Hertzian dipole antenna with a several μm photoconducting gap at the center fabricated on a semi-insulating GaAs. A large DC bias (~7.5 kV/cm) is applied across the antenna, and when carriers are photoinjected into the gap by short-pulsed laser absorption, a current transient is produced, giving rise to an output pulse of broadband low-frequency radiation. Coherent detection of the output field transient is accomplished with an optically gated antenna receiver, or by electro-optic (EO) detection. Review discussions on the generation, detection, and analysis using TTDS can be found in papers by Grischkowsky and Zhang (Grischkowsky and Katzenellenbogen, 1991; Chen et al., 2001). It was found that the spatial dependence of frequency content across the focus for the broadband source coupled with nonuniform films resulted in varying frequency dependence of the measured absorbances. This spatial variation was more severe in the all-photoconductive switch system than in the electro-optic system. With sufficiently uniform films and optimization of the uniformity in the frequency content across the focus using the EO system, we achieved consistent and quantitative absorbance measurements. Overall trends, such as temperature, hydration, and conformation dependencies were consistent between the two measurement systems and for less uniform films. The bandwidth of our systems was limited to 60 cm^{-1} for these measurements. The TTDS systems

used were enclosed in a dry nitrogen purged box to diminish THz absorption due to ambient humidity. In all cases the samples and references were mounted behind metal apertures (diameters = 4 mm) at the focus of the THz beam, (diameter <2 mm, Rayleigh range >4 mm) and the transmission was measured through repeated toggling between the reference and the sample to reduce effects due to laser and optics drift. All data shown here are of the absorbance as defined by: $Abs = -2 \, log \, |E_{sample}/E_{reference}|$, where E_{sample} ($E_{reference}$) is the field transmitted through the sample (reference). We do not discuss the phase measurements here.

In addition to the FIR measurements, a low-power tungsten-halogen beam is also directed through the sample for monitoring of the UV/Vis absorption. This allows us to assess the conformational state of the bacteriorhodopsin samples. The transmitted white light is collected and focused onto an optical fiber and analyzed using an Ocean Optics spectrometer (Dunedin, FL).

NORMAL MODE ANALYSIS

Well-known computational methods to study dynamics of biopolymers are molecular dynamics and normal mode analysis. Normal mode analysis has several advantages. It is a relatively rapid computational technique, the calculated frequencies can be compared with resonance frequencies from experimental methods such as FIR spectroscopy, and low-frequency modes can be correlated to conformation fluctuations (Brooks et al., 1995). Normal mode calculations were performed to analyze normal mode density, atomic fluctuations, and FIR spectra of WT and D96N protein in the resting state. The atomic coordinates used in the calculations were Protein Data Bank (PDB) entry 1C3W (1.55 Å resolution (Luecke et al., 1999a)) for WT and PDB entry 1C8R (2.0 Å resolution (Luecke et al., 1999b)) for D96N. Hydrogen atoms were added using InsightII 2000 (Accelrys, San Diego, CA). The protonation states of the residues were assigned assuming a pH = 7.0. The resulting net charges were +1 for Arg and Lys residues, –1 for Asp and Glu residues, and 0 for His. The residues D115 and D96 (wild-type BR) were assigned net charges of 0 (Bousche et al., 1992; Ren et al., 2001).

The crystal structure of a protein is generally inappropriate for direct harmonic analysis due to bad nonbonding contacts and unoptimized internal geometries. A normal mode calculation is usually carried out on an energy minimum (Janezic and Brooks, 1995). A series of energy minimizations was carried out to satisfy this requirement. This was done using cycles of steepest descent and adopted basis Newton Raphson algorithm (Brooks et al., 1983). Harmonic constraints were applied on the protein backbone, and were progressively reduced at each cycle. Finally, the constraints were removed and the system was minimized until the energy gradient was 10^{-6} kcal/Å. The nonbonded interactions were truncated at 13 Å and van der Waals interactions switched between 10 Å and 12 Å.

Normal modes were obtained using iterative diagonalization in a mixed basis set, previously developed for large molecular systems (Mouawad and Perahia, 1993). This method has been applied to hemoglobin and phosphoglyc-
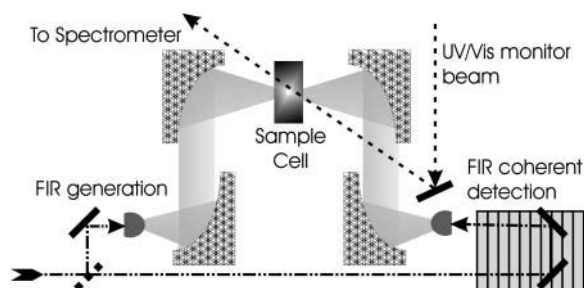

FIGURE 2 Schematic of terahertz time domain spectroscopy system with coincident UV/Vis absorbance monitoring for the FIR absorbance measurements. The dashed-dot-dot line represents the NIR light that is used to generate and detect the FIR pulses, the gray line represents the FIR, and the dashed line represents the light from a tungsten-halogen lamp used for monitoring the UV/Vis absorption.

erate kinase (Mouawad and Perahia, 1996) (Guilbert et al., 1996; Perahia and Mouawad, 1995). It uses an iterative procedure that converges from a set of initial trial modes to the refined lowest frequency ones within a given error tolerance.

The program CHARMM27 with CHARMM22 parameter set (Brooks et al., 1983; MacKerell et al., 1998) was used for all energy minimizations and normal mode analysis. A histogram of the calculated normal mode frequencies is shown in Fig. 3. The first 403 modes were calculated. There were no negative frequencies in the calculation, and the six modes corresponding to translational and rotational motion were all present. There are no significant differences between the normal mode density of WT and D96N.

The theoretical absorption spectra of WT and D96N were calculated. For each mode ν we define the state $|n\rangle$ with collective vibrational energy $h\nu(n + 1/2)$. The absorbance for a transition from n to $n + 1$ can be estimated from the dipole derivative associated with each mode (Person and Zerbi, 1982). The IR absorbance, A_{ir}, of a vibrating normal coordinate, Q_ν, of a molecule is proportional to the square of the transition dipole moment, which for linear response can be approximated by the derivative of the molecular dipole moment with respect to Q_ν:

$$I_{ir} = A\bar{\nu}(n_\nu - n_{\nu+1})(\nu + 1)\left(\frac{d\bar{\mu}}{dQ_k}\right)^2, \qquad (1)$$

where $\bar{\mu}$ is the dipole moment, N_n is the density of molecules with quantum number n, and B is a constant (Palmo and Krimm, 1998). We note that we use a fixed charge model here whereas Palmo and Krimm use a polarizable force field. Using the Boltzmann distribution, N_n can be expressed as:

$$n_\nu = ne^{-hc\bar{\nu}(\nu+1/2)/kT} / \sum_\nu e^{-hc\bar{\nu}(\nu+1/2)/kT}, \qquad (2)$$

where N is the total number of molecules per unit volume(Polavarapu, 1998). In the harmonic approximation, with equal energy level spacing for a displacement vector, Eq. 1 is summed over all n, and the intensity is therefore temperature independent. However, for proteins, the conformational potential is highly anharmonic and thus we consider only the transition of $n = 0' \rightarrow n = 1$ (Roitberg et al., 1995). Fig. 4 shows the theoretical absorbance spectra of WT and D96N for $T = 300$ K.

From the calculated eigenfrequencies and eigenvectors, statistical measures of motion can be derived. These measures are useful to discover which residues move the most and which remain stationary. The atomic fluctuations from a harmonic approximation is given by

$$\langle \Delta x_k^2 \rangle = k_B T \sum_{i=1}^{3N-6} \frac{|y_{ki}|^2}{M_k \omega_i^2}, \qquad (3)$$

where M_k is the atomic mass, i spans the modes of interest, y is the eigenvector, and k corresponds to the component of motion of an atom in the x, y, or z direction (Brooks et al., 1995). Fig. 5 shows the average rms fluctuations of all atoms along each mode. It shows which modes contribute most significantly to the atomic fluctuations, which is a measure of the overall mobility of WT and D96N. It is seen that rms fluctuations are very large for the first few modes and indicates that low-frequency modes induce most of the large-scale motion. Conversely, high-frequency modes result in very small atomic fluctuations.

EXPERIMENTAL RESULTS AND DISCUSSION

The room temperature, 80% r.h. absolute absorbances, are shown in Fig. 6 from WT and D96N samples. Both samples
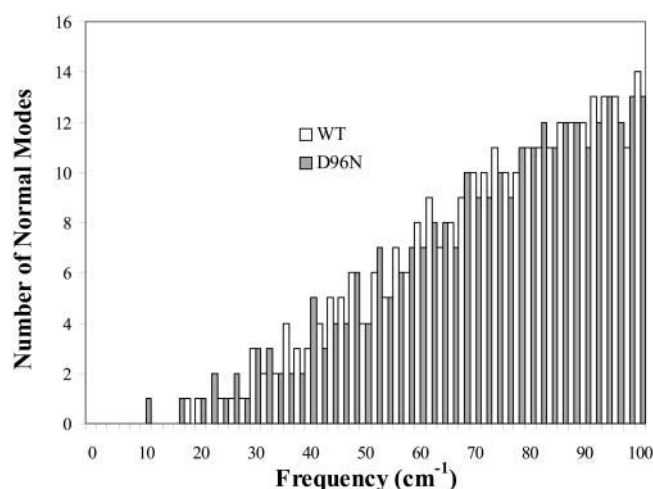

FIGURE 3 Density of normal modes calculated with CHARMM for bacteriorhodopsin molecules: wild-type (PDB 1C3W (Luecke et al., 1999a)) and D96N (PDB 1C8R (Luecke et al., 1999b)). No bound waters are included in the calculation. Bin size is 2 cm^{-1}. See text for details.
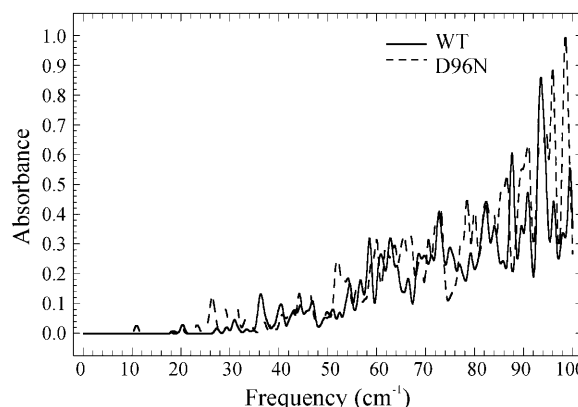

FIGURE 4 FIR absorbance calculated using CHARMM for wild-type and D96N bacteriorhodopsin. The calculation uses the full normal mode spectra shown in Fig. 3 along with calculated dipole moment change for each mode. Only transitions from $n = 0$ to $n = 1$ of the harmonic modes are included.
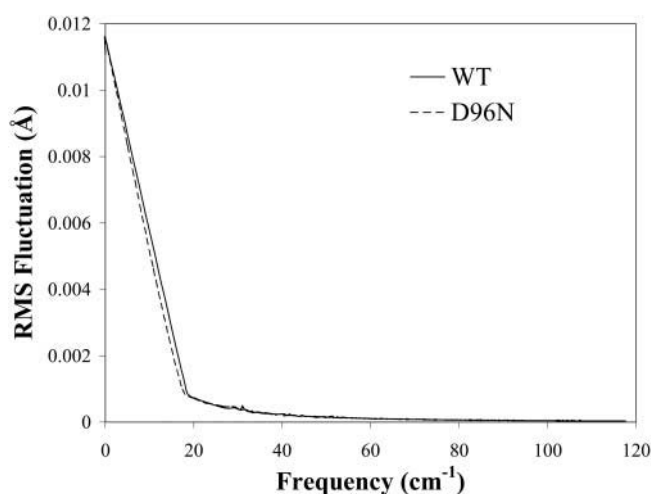
FIGURE 5 Average rms fluctuations versus frequency for WT and D96N bacteriorhodopsin for the vibrational modes shown in Fig. 3 and determined using CHARMM. The large amplitude fluctuations are concentrated in the low-frequency region.

had $A_{568} = 2.7$, and great care was taken to ensure film thickness uniformity and THz frequency content uniformity over the entire illuminated area. The absorbance for both appears nearly linear over the frequency range, without the narrow band features shown in the calculated spectra in Fig. 4. Xie et al. (2002) measured a lifetime of >500 ps for 115 cm^{-1} conformation mode for BR at room temperature. This
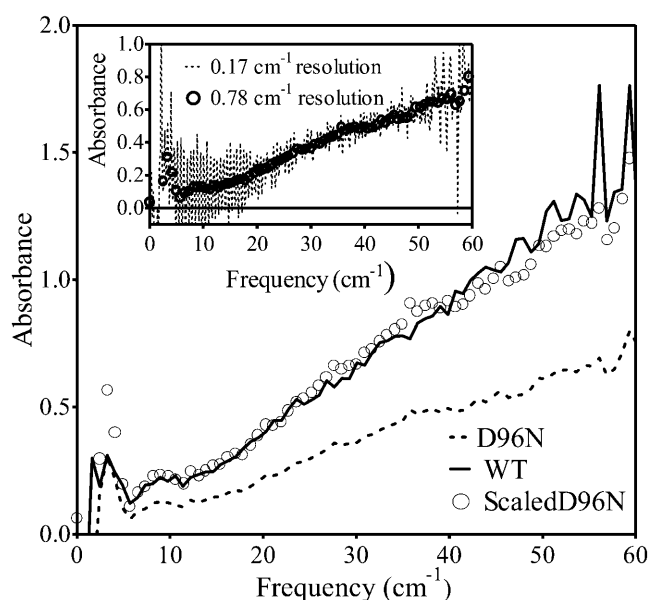

FIGURE 6 Comparison of FIR absorption of D96N mutant and WT bacteriorhodopsin thin films at room temperature 80% r.h. The two samples have $A_{568} = 2.7$. Notice that if the mutant is scaled by factor of 2, it nearly overlays that of WT. The inset shows a high resolution measurement of the WT sample. While the absorption shows a strong etalon due to the substrate, no individual collective modes as shown in the calculated spectra of Fig. 4 can be identified. See text for discussion.

lifetime implies a homogeneous broadening of <0.07 cm^{-1} and our calculations give a mode spacing of 0.25 cm^{-1}; still no narrow features are observed even at resolutions of 0.17 cm^{-1} as seen in the inset of Fig. 6. The results can be reconciled by noting that the calculated spectra and mode spacing assumed a specific minimized structure. A macroscopic room temperature sample will have an assembly of minima, with slightly varying spectra thus obscuring specific modes. This result then suggests that specific collective mode identification requires either single molecule spectroscopy or nonlinear measurements to preferentially excite a uniform population. We note that unlike the more familiar interatomic vibrational spectroscopy such as the C-C stretch within the polypeptide chain, FIR absorbance probes large-scale collective motion, and thus is strongly dependent on the global conformation.

As can be seen in the figure, the D96N absorbance is somewhat less than the WT; however, scaling the measurement by a factor of 1.8, the absorbances nearly overlay exactly. Der and Keszthelyi (2001) have measured ground-state dipole moments of $\mu_{WT} = -1.30 \times 10^{-23}$ Cm and $\mu_{D96N} = -1.00 \times 10^{-23}$ Cm. However, this is not sufficient to explain the difference in the oscillator strengths observed. For all samples measured, the relative values of the room temperature FIR absorbance directly scale with the ground-state A_{568}.

Comparing the measured absorbance with the calculated spectra in Fig. 4, we see that for this first attempt to compare experimental and theoretical spectra in the THz region, and the theoretical calculations show only general agreement with the profiles observed experimentally. The overall calculated frequency dependence of the absorbances shown in Fig. 4 is in fairly good agreement with the experiment; however, they do not reproduce the observation that WT has higher absorptivity than D96N in this region. Some very low-frequency (below 10 cm^{-1}) modes observed experimentally were absent in the theoretical spectra. Some of these may be due to inorganic cation resonances, which dominate the microwave region below 40 GHz (Birge et al., 1996). Differences in the frequencies and intensities obtained between the calculations and experiment can be attributed to the fact that real frequencies are strongly influenced by anharmonic effects and solvent damping (Hinsen, 1998). Classical force fields are not designed to address these issues, and experiments like this may help to improve these force field calculations. Our intensity calculations assume harmonic potentials, only considered transitions from $n = 0$ to $n = 1$ of the harmonic modes, and do not include bound water. In addition, the use of a classical force field and standard atom charges will invariably lead to errors in both band position and intensities.

One might have anticipated that the nature of very low-frequency modes might be amenable to semiclassical analysis. Although this might ultimately be true, explicit handling of water molecules will be required. It is also likely
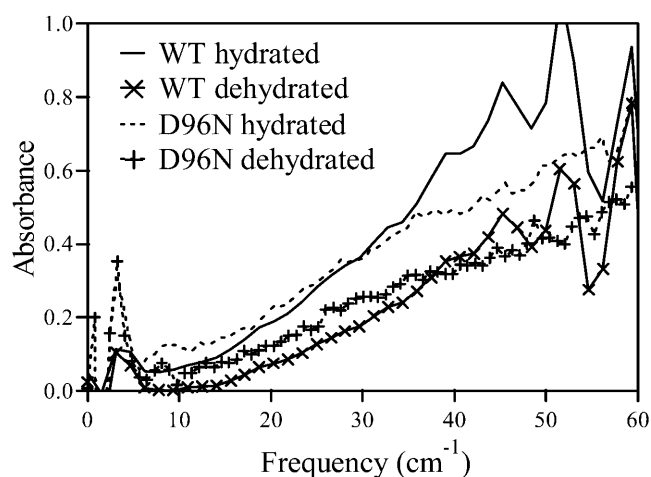
FIGURE 7 Hydration dependence of the FIR absorbance for WT and D96N bacteriorhodopsin thin films. All measurements were at room temperature with hydrated (dehydrated) spectra taken at 80% r.h. (<5% r.h) respectively. For this figure and Figs. 8 and 9, the frequency-dependent features appearing between 50 and 60 cm^{-1} are considered artifacts arising from nonuniformity of the films and spatial dependence in the THz frequency content at the focus (see text).

conformation were mainly performed using the photoconductive switch detection system and were more effected by the spatial nonuniformity of both the frequency distribution in the FIR focus and the thin film samples' thickness variation, so the frequency dependence of the absorbances appears slightly different than those in Fig. 6. All trends presented for the hydration and conformational measurements were observed for all samples measured.

The hydration dependence is shown in Fig. 7. We measured three different hydration levels, 80% r.h., 30% r.h., and <5% r.h. The 80% and 30% r.h. data overlay for all samples measured (80% r.h. is shown in the figure), whereas when the cell was purged with dry nitrogen gas, the net absorbance decreased in a uniform way. The change in absorbance as a function of hydration may come from a variety of effects. We note that at 80% r.h., the hydration was not sufficient for liquid condensation on the sample or substrate. Possible effects include mass loading, increased intramolecular coupling mediated by interior water molecules, and collective modes of interior water clusters. At 80% r.h. there are ~180 H_2O molecules/BR molecule (Varo and Keszthelyi, 1983). Effective mass loading is then expected to shift spectrum by ~6%; however, we see a somewhat more dramatic effect. Thus most likely the observed increased absorption with water content arises from increased intramolecular coupling or collective modes of interior water clusters. INS measurements show a comparable change in scattering amplitude for the same hydration change (Ferrand et al., 1993).

We will now discuss the conformational dependence measurements. The FIR absorbances are shown in Figs. 8 and 9, and the UV/Vis absorbance change upon illumination is shown in Fig. 10. Fig. 8 shows that for the WT samples, the higher frequency FIR absorption decreases as the temperature is lowered, in good agreement with temperature-dependent INS measurements (Ferrand et al., 1993;

that the coupling of the low-frequency modes with the phonon structure of the semicrystalline purple membrane lattice may contribute to the FIR profile. Studies on the protein monomer are planned to test this hypothesis. If this is true, the degree of difficulty of the theoretical calculations increases by at least one order of magnitude. Nevertheless, the calculations do provide a perspective on the origins of the unexpectedly large difference in the THz spectrum of WT versus D96N.

The absolute absorbances shown in Fig. 6 were determined by extreme care in preparing uniform films and optimizing spatial uniformity in the FIR focus for the EO detection system. The measurements on hydration and
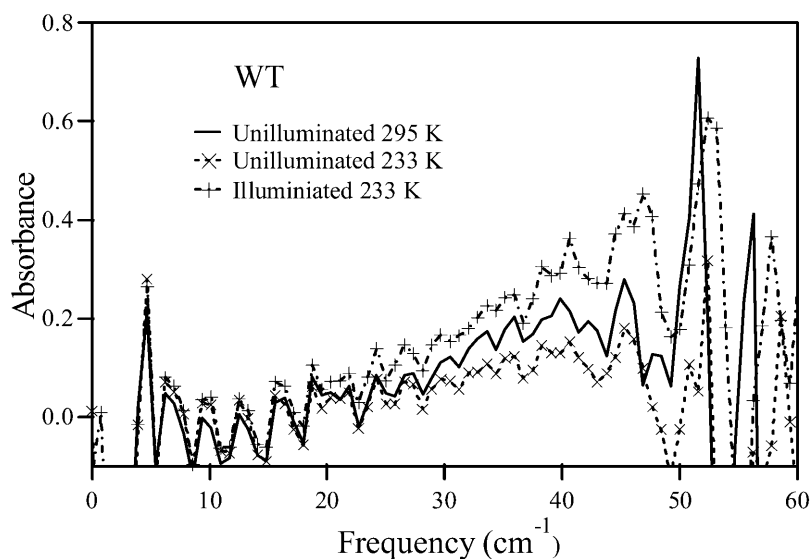

FIGURE 8 Temperature and conformation dependence of a thin film of WT bacteriorhodopsin, measured at r.h. = 80%. The solid line shows the 293 K data. The X with the dashed line through it shows the 233 K data, unilluminated and still in the BR state, or resting state. There is a decrease in the FIR absorbance as increasing frequencies compared to that of the room temperature data. The plus sign with the dotted line through it shows the 233 K data illuminated with M-state content shown by UV/Vis absorption as shown in Fig. 10 a. There is an overall increase in FIR absorbance above that of both the 233 K unilluminated data and the 295 K data. A 3 cm^{-1} period etalon is observed that was not entirely removed by the reference.
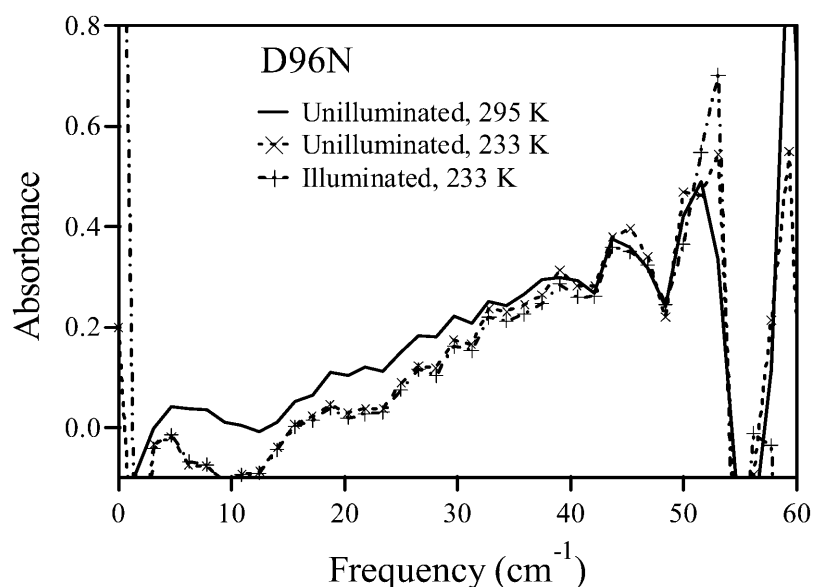
FIGURE 9 Temperature and conformation dependence of a thin film of D96N bacteriorhodopsin, measured at r.h. = 80%. The solid line shows the 293 K data. The X with the dashed line through it shows the 233 K data, unilluminated and in the resting state. There is a decrease in the FIR absorbance at lower frequencies compared to that of the room temperature data. The plus sign with the dotted line through it shows the 233 K data illuminated with M-state content shown by UV/Vis absorption as shown in Fig. 10 *b*. There is no change in the FIR absorption observed for the M state of D96N.

Zaccai, 2000). This temperature dependence can be interpreted as the changing accessibility of vibrational modes as a function of temperature due to the changing occupation of the lower lying states of the anharmonic potential (Austin et al., 1975). Conceptually, the molecule has a ladder of conformational vibrational modes corresponding to the curvature of the potential. For an anharmonic potential, the spacing between modes changes as energy increases. In the case of WT, as the temperature increases, the absorption at higher frequency increases. This suggests that the occupation of higher energy states at the higher temperature allows access to higher frequency vibrational modes,

suggesting an increasing curvature with energy. In contrast, Fig. 9 shows that the mutant's low frequency absorption increases with temperature, suggesting a decreasing curvature with energy. For both the WT and D96N, we see a negative absorbance at the lowest frequencies when the samples are cooled, which is most likely due to a referencing artifact.

Upon illumination, BR undergoes a conformational change. This change in UV/Vis absorption is shown in Fig. 10, where $\Delta A = A_{\text{light}} - A_{\text{dark}}$. For the WT sample, the FIR absorbance increases upon this conformational change. WT sample returned to the low temperature FIR absorbance
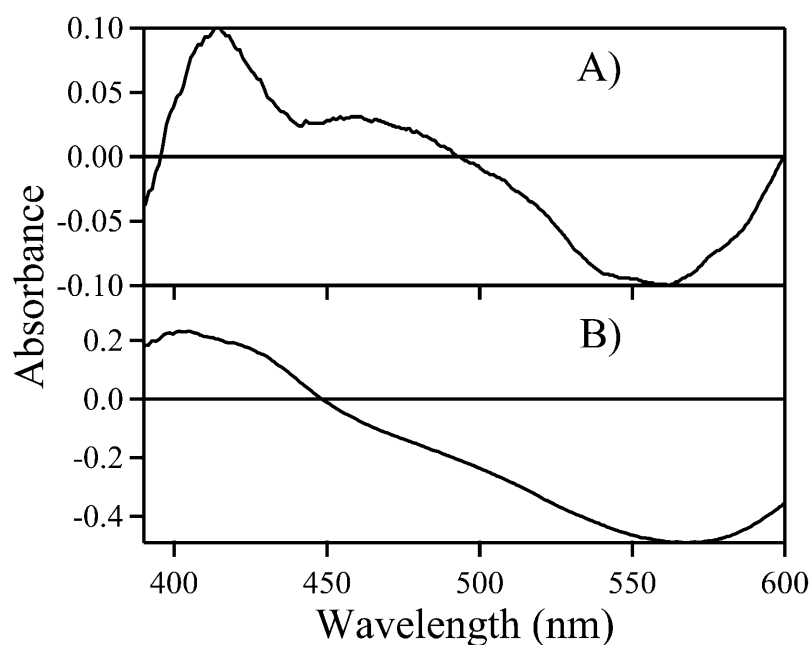

FIGURE 10 UV/Vis absorbance referenced to unilluminated ground-state samples for FIR conformational dependence shown in Figs. 8 and 9. (*A*) Wild-type and (*B*) D96N mutant thin films at 233 K. The spectra demonstrate the increase in absorption at 410 nm corresponding to the M state capture and a decrease in the 568 nm line corresponding to decrease in the ground-state population. Note that for the WT sample, the decrease in the ground state does not correspond to only the two-state occupancy and the additional peak at ~490 nm as well as an inflection at ~560 nm suggesting possible N and P content.

with illumination of $\lambda < 480$ nm. The increase in FIR absorbance with $\lambda > 480$ nm illumination was seen for all WT samples. On the other hand, there is no change in the FIR absorbance for D96N upon illumination. The change in the FIR absorption can come about either due to a change in the dipole moment or a change in the normal mode density of states. A large conformational change for BR occurs in the L → M transition (Dencher et al., 1989). Electrical measurements on oriented BR membranes show that the change in dipole moment from ground state to M is nearly identical for WT and D96N (Der and Keszthelyi, 2001). This would suggest that the observed increase in FIR absorbance for WT with conformational change may be due to an increase in the normal mode density and that this increase in normal mode density is greater in WT than that for D96N. Since it is the low frequency modes that have the largest amplitude fluctuations, this increase in normal mode density at low frequencies suggests greater conformational flexibility, which would agree with the shorter photocycling time for WT.

We note that although we expect that most of the conformational change to be in the M state, and thus any change in the FIR absorbance to be associated with that intermediate, the UV/Vis spectra suggest that the amount of M content for the WT is less than that for the D96N sample, and the WT sample may also have N and possibly P intermediates as well. Thus it is possible that the FIR absorbance increase observed for the WT is due to the other intermediates. Using the TTDS system, we can perform time-resolved measurements, thus follow in time the change in the FIR absorbance for each intermediate, verified by the secondary UV/Vis absorbance probe.

CONCLUSIONS

The FIR absorbance for ground-state wild-type bacteriorhodopsin and D96N agrees well with normal mode calculations and electric dipole measurements, but the calculated intensity suggests that anharmonicity needs to be included for accurate calculated absorbances. The absorbance is broad and increasing with frequency without any specific mode dominating, with the D96N having a smaller absorbance associated with its smaller dipole moment. The temperature dependence of the FIR absorbance suggests that the anharmonicity of the conformational potential can be quantified, and requires more thorough measurements of this temperature dependence. Finally, FIR absorbance is conformation dependent for the WT, and apparently conformation independent for the mutant. This is the first observation of a conformational change through the conformational vibrational mode spectrum. However it is not clear if the change in absorbance is associated with the M-state intermediate, and future time-resolved studies of the THz response as a function of photo-initiated conformational change should resolve this question.

REFERENCES

Austin, R. H., K. W. Beeson, L. Eisenstein, H. Frauenfelder, and I. C. Gunsalus. 1975. Dynamics of ligand binding to myoglobin. *Biochemistry*. 14:5355–5373.

Birge, R. R., D. S. K. Govender, K. C. Izgi, and E. H. L. Tan. 1996. Role of calcium in the proton pump or bacteriorhodopsin. Microwave evidence for a cation-gated mechanism. *J. Phys. Chem.* 100:9990–10004.

Bousche, O., S. Sonar, M. Krebs, H. Khorana, and K. Rothschild. 1992. Time-resolved Fourier transform infrared spectroscopy of the bacteriorhodopsin mutant Tyr-185→Phe: Asp-96 reprotonates during O formation; Asp-85 and Asp-212 deprotonate during O decay. *Photochem. Photobiol.* 56:1085–1095.

Brooks, B. R., R. E. Bruccoleri, B. D. Olafson, D. J. States, S. Swaminathan, and M. Karplus. 1983. CHARMM: a program for macromolecular energy, minimization, and dynamics calculations. *J. Comput. Chem.* 4:187–217.

Brooks, B. R., D. Janezic, and M. Karplus. 1995. Harmonic analysis of large systems. *J. Comput. Chem.* 16:1522–1542.

Brooks, C. L., M. Karplus, and B. M. Pettitt. 1988. Proteins: A Theoretical Perspective of Dynamics, Structure, and Thermodynamics. John Wiley & Sons, New York.

Brucherseifer, M., M. Nagel, P. H. Bolivar, H. Kurz, A. Bosserhoff, and R. Buttner. 2000. Label-free probing of the binding state of DNA by time-domain terahertz sensing. *Appl. Phys. Lett.* 77:4049–4051.

Chen, Q., M. Tani, Z. P. Jiang, and X.-C. Zhang. 2001. Electro-optic transceivers for terahertz-wave applications. *J. Opt. Soc. Am. B.* 18:823–831.

Dencher, N. A., D. Dresselhaus, G. Zaccai, and G. Buldt. 1989. Structural changes in bacteriorhodopsin during proton translocation revealed by neutron diffraction. *Proc. Natl. Acad. Sci. USA.* 86:7876–7879.

Der, A., and L. Keszthelyi. 2001. Charge motion during the photocycle of bacteriorhodopsin. *Biochemistry.* 66:1234–1248.

Diehl, M., W. Doster, W. Petry, and H. Schober. 1997. Water-coupled low-frequency modes of myoglobin and lysozyme observed by inelastic neutron scattering. *Biophys. J.* 73:2726–2732.

Doster, W., S. Cuszck, and W. Petry. 1989. Dynamical transition of myoglobin revealed by inelastic neutron scattering. *Nature.* 337:754–756.

Ferrand, M., A. J. Dianoux, W. Petry, and G. Zaccai. 1993. Thermal motions and function of bacteriorhodopsin in purple membranes: effects of temperature and hydration studies by neutron scattering. *Proc. Natl. Acad. Sci. USA.* 90:9668–9676.

Genzel, L., L. Santo, and S. C. Shen. 1984. Far-infrared spectroscopy of biomolecules. *In* Spectroscopy of Biological Molecules. C. Sandory and T. Theophanides, editors. D. Reidel, Boston. 609–619.

Grischkowsky, D., and N. Katzenellenbogen. 1991. Femtosecond pulses of terahertz radiation: physics and applications. *OSA Proceedings on Picosecond Electronics and Optoelectronics.* OSA, Washington, DC. 9–14.

Guilbert, C., F. Pecorari, D. Perahia, and L. Mouawad. 1996. Low frequency motions in phosglycerate kinase. A normal mode analysis. *Chem. Phys.* 204:327–336.

Han, P. Y., G. C. Cho, and X.-C. Zhang. 2000. Time-domain trans-illumination of biological tissues using THz pulses. *Opt. Lett.* 25:242–244.

Hinsen, K. 1998. Analysis of domain motions by approximate normal mode calculations. *Proteins.* 33:417–429.

Janezic, D., and B. R. Brooks. 1995. Harmonic analysis of large systems. II. Comparison of different protein models. *J. Comput. Chem.* 16:1543–1553.

Kusnetzow, A., D. L. Singh, C. H. Martin, I. Barani, and R. R. Birge. 1999. Nature of the chromophore binding site of bacteriorhodopsin. The potential role of Arg[82] as a principal counterion. *Biophys. J.* 76:2370–2389.

Lanyi, J., and A. Pohorille. 2001. Proton pumps: mechanism of action and applications. *Trends Biotechnol.* 19:140–144.

Lanyi, J. K. 1999. Bacteriorhodopsin. *Int. Rev. Cytol.* 187:161–202.

Lindsay, S. M., S. A. Lee, J. W. Powell, T. Weidlich, C. Demarco, G. D. Lewen, N. J. Tao, and A. Rupprecht. 1988. The origin of the A to B transition in DNA fibers and films. *Biopolymers.* 27:1015–1043.

Lisy, V., P. Miskovsky, B. Brutovsky, and L. Chinsky. 1997. Internal DNA modes below 25 cm^{-1}: a resonance Raman spectroscopy observation. *J. Biomol. Struct. Dyn.* 14:517–523.

Longbottom, C., D. A. Crawley, B. E. Cole, D. D. Arnone, V. P. Wallace, and M. Pepper. 2002. Potential Uses of Terahertz Pulse Imaging in Dentistry: Caries and Erosion Detection. SPIE Press, San Jose, CA.

Luecke, H., B. Schobert, H. T. Richter, J. P. Cartailler, and J. K. Lanyi. 1999a. Structure of bacteriorhodopsin at 1.55 Å resolution. *J. Mol. Biol.* 291:899–911.

Luecke, H., B. Schobert, H.-T. Richter, J.-P. Cartailler, and J. K. Lanyi. 1999b. Structural changes in bacteriorhodopsin during ion transport at 2 Å resolution. *Science.* 286:255–261.

MacKerell, A. D., Jr., D. Bashford, M. Bellott, R. L. Dunbrack, J. D. Evanseck, M. J. Field, S. Fischer, J. Gao, H. Guo, S. Ha, D. Joseph-McCarthy, L. Kuchnir, K. Kuczera, F. T. K. Lau, C. Mattos, S. Michnick, T. Ngo, D. T. Nguyen, B. Prodhom, W. E. Reiher, III, B. Roux, M. Schlenkrich, J. Smith, R. Stote, J. Straub, M. Watanabe, J. Wiórkiewicz-Kuczera, D. Yin, and M. Karplus. 1998. All-atom empirical potential for molecular modeling and dynamics studies of proteins. *J. Phys. Chem. B.* 102:3586–3616.

Markelz, A. G., A. Roitberg, and E. J. Heilweil. 2000. Pulsed terahertz spectroscopy of DNA, bovine serum albumin and collagen between 0.06 and 2.00 THz. *Chem. Phys. Lett.* 320:42–48.

McIntosh, A. R., and F. Boucher. 1991. Photochemically induced charge separation occurring in bacteriorhodopsin: detection by time-resolved dielectric loss. *Biophys. J.* 60:1–7.

Mouawad, L., and D. Perahia. 1993. Diagonalization in a mixed basis: a method to compute low-frequency normal modes for large macromolecules. *Biopolymers.* 33:599–611.

Mouawad, L., and D. Perahia. 1996. Motions in hemoglobin studied by normal mode analysis and energy minimizations. Evidence for the existence of tertiary T-like, quaternary R-like intermediate structures. *J. Mol. Biol.* 258:393–410.

Nagel, M., P. H. Bolivar, M. Brucherseifer, H. Kurz, A. Bosserhoff, and R. Buttner. 2001. Integrated THz technology for label-free genetic diagnostics. *Appl. Phys. Lett.* 80:154–156.

Oesterhelt, D., and W. Stoeckenius. 1974. Isolation of the cell membrane of halobacterium halobium and its fractionation into red and purple membrane. *Methods Enzymol.* 31:667–678.

Palmo, K., and S. Krimm. 1998. Electrostatic model for infrared intensities in a spectroscopically determined molecular mechanics force field. *J. Comput. Chem.* 19:754–768.

Perahia, D., and L. Mouawad. 1995. Computation of low-frequency normal modes in macromolecules: improvements to the method of diagonaliza-

tion in a mixed basis and application to hemoglobin. *Comput. Chem.* 19:241–246.

Person, W. B., and G. Zerbi. 1982. Vibrational Intensities in Infrared and Raman Spectroscopy. Elsevier Scientific Publishing, Amsterdam, The Netherlands.

Polavarapu, P. L. 1998. Vibrational Spectra: Principles and Applications with Emphasis on Optical Activity. Elsevier Science, New York.

Powell, J. W., G. S. Edwards, L. Genzel, F. Kremer, A. Wittlin, W. Kubasek, and W. Peticolas. 1987. Investigation of far-infrared vibrational modes in polynucleotides. *Phys. Rev. A.* 35:3929–3939.

Powell, J. W., W. L. Peticolas, and L. Genzel. 1991. Observation of the far-infrared spectrum of five oligonucleotides. *J. Mol. Struct.* 247:107–118.

Ren, L., C. H. Martin, K. J. Wise, N. B. Gillespie, H. Luecke, J. K. Lanyi, J. L. Spudich, and R. R. Birge. 2001. Molecular mechanism of spectral tuning in sensory rhodopsin II. *Biochemistry.* 40:13906–13914.

Roitberg, A., R. B. Gerber, R. Elber, and M. A. Ratner. 1995. Anharmonic wave functions of proteins: quantum self-consistent field calculations of BPTI. *Science.* 268:1319–1322.

Sass, H. J., I. W. Schachowa, G. Rapp, M. H. J. Koch, D. Oesterhelt, N. A. Denscher, and G. Buldt. 1997. The tertiary structural changes in bacteriorhodopsin occur between M states: X-ray diffraction and Fourier transform infrared spectroscopy. *EMBO J.* 16:1484–1491.

Stuart, J. A., and R. R. Birge. 1996. Characterization of the primary photochemical events in bacteriorhodopsin and rhodopsin. *In* Biomembranes. A. G. Lee, editor. JAI Press, London. 33–140.

Urabe, H., Y. Sugawara, M. Ataka, and A. Rupprecht. 1998. Low-frequency Raman spectra of lysozyme crystals and oriented DNA films: Dynamics of crystal water. *Biophys. J.* 74:1533–1540.

Varo, G., and L. Keszthelyi. 1983. Photoelectric signals from dried oriented purple membranes of halobacterium halobium. *Biophys. J.* 43:47–51.

Walther, M., B. Fischer, M. Schall, H. Helm, and P. U. Jepsen. 2000. Far-infrared vibrational spectra of all-trans, 9-cis and 13-cis retinal measured by THz time-domain spectroscopy. *Chem. Phys. Lett.* 332:389–395.

Weidlich, T., and S. M. Lindsay. 1988. Raman study of the low-frequency vibrations of polynucleotides. *J. Phys. Chem.* 92:6479–6482.

Weidlich, T., S. M. Lindsay, and A. Rupprecht. 1987. The optical properties of Li- and Na-DNA films. *Biopolymers.* 26:439.

Weidlich, T., S. M. Lindsay, Q. Rui, A. Rupprecht, W. L. Peticolas, and G. A. Thomas. 1990a. A Raman study of low-frequency intrahelical modes in A-DNA, B-DNA, and C-DNA. *J. Biomol. Struct. Dyn.* 8:139–171.

Weidlich, T., J. W. Powell, L. Genzel, and A. Rupprecht. 1990b. Counterion effects on the far-infrared vibrational-spectra of poly(ri). poly(rC). *Biopolymers.* 30:477–480.

Wittlin, A., L. Genzel, F. Kremer, S. Haseler, and A. Poglitsch. 1986. Far-infrared spectroscopy on oriented films of dry and hydrated DNA. *Phys. Rev. A.* 34:493–500.

Woolard, D. L., T. Koscica, D. L. Rhodes, H. L. Cui, R. A. Pastore, J. O. Jensen, J. L. Jensen, W. R. Loerop, R. H. Jacobsen, D. Mittleman, and M. C. Nuss. 1997. Millimeter wave-induced vibrational modes in DNA as a possible alternative to animal tests to probe for carcinogenic mutations. *J. Appl. Toxicol.* 17:243–246.

Xie, A., A. F. van der Meer, and R. H. Austin. 2002. Excited-state lifetimes of far-infrared collective modes in proteins. *Phys. Rev. Lett.* 88:018102.

Zaccai, G. 2000. How soft is a protein? A protein dynamics force constant measured by neutron scattering. *Science.* 288:1604–1607.